

Time-Parameterized Convolutional Neural Networks for Irregularly Sampled Time Series

Chrysoula Kosma
 École Polytechnique, IP Paris
 France
 kosma@lix.polytechnique.fr

Giannis Nikolentzos
 École Polytechnique, IP Paris
 France
 nikolentzos@lix.polytechnique.fr

Michalis Vazirgiannis
 École Polytechnique, IP Paris
 France
 mvazirg@lix.polytechnique.fr

Abstract

Irregularly sampled multivariate time series are ubiquitous in several application domains, leading to sparse, not fully-observed and non-aligned observations across different variables. Standard sequential neural network architectures, such as recurrent neural networks (RNNs) and convolutional neural networks (CNNs), consider regular spacing between observation times, posing significant challenges to irregular time series modeling. While most of the proposed architectures incorporate RNN variants to handle irregular time intervals, convolutional neural networks have not been adequately studied in the irregular sampling setting. In this paper, we parameterize convolutional layers by employing time-explicitly initialized kernels. Such general functions of time enhance the learning process of continuous-time hidden dynamics and can be efficiently incorporated into convolutional kernel weights. We, thus, propose the time-parameterized convolutional neural network (TPCNN), which shares similar properties with vanilla convolutions but is carefully designed for irregularly sampled time series. We evaluate TPCNN on both interpolation and classification tasks involving real-world irregularly sampled multivariate time series datasets. Our experimental results indicate the competitive performance of the proposed TPCNN model which is also significantly more efficient than other state-of-the-art methods. At the same time, the proposed architecture allows the interpretability of the input series by leveraging the combination of learnable time functions that improve the network performance in subsequent tasks and expedite the inaugural application of convolutions in this field.

1 Introduction

Time series arise naturally in many contexts including quantitative finance, astrophysics and medicine, just to name a few. Recently, there is a growing interest in applying machine learning techniques to time series data. Besides time series forecasting, which has been extensively studied for decades [7], other tasks have also emerged recently such as time series classification [12] and generation [8].

Time series are constructed from real-world data and usually several of their observations are missing or are subject to noise. This is mainly due to irregular sampling and is common in different types of data including medical records, network traffic, and astronomical data. Unfortunately, the most successful machine learning models in sequential modeling, namely recurrent neural networks (RNNs) and convolutional neural networks (CNNs) cannot properly handle such irregularly sampled time series data. Indeed, those models treat observations successively and assume an equidistant sampling scheme. Thus, time series data that

exhibits variable gaps between consecutive time points pose a significant challenge to such conventional deep learning architectures. A naive approach to deal with the above problem would be to drop some observations such that the distance between consecutive (remaining) observations is fixed. However, this would increase data sparsity, thus leading to poorly defined latent variables. A more prominent approach would be to first apply some imputation method to replace missing values with estimated values, and then to use the standard models which assume an equidistant sampling scheme. In fact, several recent approaches build on the above idea [3, 9]. However, this could potentially result in a loss of information and a violation of the underlying dynamics.

Recently, there has been an increasing interest in effectively capturing the continuous dynamics of real-world sparse and irregular multivariate time series. Most studies have extended RNNs to continuous-time hidden dynamics defined by ordinary differential equations (ODEs) [4, 24]. The effectiveness of Convolutional Neural Networks (CNNs) [15] as an alternative to recurrent architectures has been established, as long as the input dependencies that are essential fall within the memory horizon of the network. CNNs are based on parallel computations and thus are more efficient, contrary to the training instability and gradient problems of RNNs that employ back-propagation through time [34]. However, since discrete convolutions learn independent weights for each time step in the kernel range, they do not directly capture the time irregularities. Efforts for the continuous implementation of convolutional kernels have targeted 3D data [25, 33] and recently, sequences [23]. The proposed continuous convolution for sequential data [23], CKConv, parameterizes the kernel values using a multi-layer perception (MLP) on the relative positions $\{\Delta_{\tau_i}\}$ of the observations, followed by a periodic activation function [29]. In contrast to [23] that take advantage of periodic activations, our layer can be constructed employing any predefined set of continuous functions and be followed by any activation, while using significantly fewer learnable parameters, since a single feed-forward layer is used for the parameterization of the convolutional kernel.

Following the above line of research, in this paper, we develop a new model, so-called *Time-Parameterized Convolutional Neural Network* (TPCNN), which generalizes the standard CNN model to irregularly sampled time series. To achieve that, we replace the fixed kernels of CNNs with kernels whose values are parameterized both by time and by trainable variables. Thus, instead of keeping the kernel weights fixed over the whole time series length, we use different functions (e.g., linear, sinusoidal) to produce the kernels that will be convolved with each patch of the time series. Therefore, kernels can be seen as continuous functions of time, and the proposed TPCNN model can naturally learn continuous latent representations of irregular time series. Furthermore, the use of the aforementioned functions improves the explainability of the proposed model. We combine our time-parameterized convolutions with vanilla convolutions by stacking them in a deep encoder module. The proposed TPCNN model is evaluated in the tasks of time series classification and time series interpolation. Our experiments demonstrate that the proposed model performs comparably to state-of-the-art methods. The main contributions of the paper are summarized as follows:

- (i) Generalizing conventional, fixed convolutional kernels to time functions, that increase their representational power and still leverage properties of convolutions (e.g., locally aggregated information, fast training).
- (ii) Enabling the application and proving the efficiency of deep stacked convolutions in the irregular sampling setting.
- (iii) Achieving high-performance results in interpolation and classification of irregularly sampled benchmark datasets, which are comparable to other state-of-the-art methods.

2 Related Work

The long-standing challenge in multivariate irregular time series modeling has led to the development of various neural network architectures that explicitly handle such time-dependent peculiarity.

One strategy suggests dividing the timeline into equal intervals, filling in missing data, and then using a Recurrent Neural Network (RNN) on the imputed inputs. Using a weighted average between the empirical

mean and the previous observation to perform imputation has also been proposed [3]. Alternative methods for imputation include the use of Gaussian processes [9], or generative adversarial networks [16] prior to running the RNN on time-discretized inputs. The interpolation-prediction network [26] employs semi-parametric RBF interpolation layers for the interpolation of irregular multivariate time series against a set of reference time points. Multi-directional RNNs (M-RNN) combine past and future observations for each timestamp [36]. A set function-based approach for classifying time series with irregularly sampled and unaligned observations is another line of work presented in [11].

An alternative approach to temporal discretization for handling irregularly sampled data employs models that can directly process such time series. Several methods with modifications of gated recurrent unit networks (GRUs) [5] and Long Short-term Memory networks (LSTMs) [10] have been proposed. More specifically, many RNN variants are based on GRUs [3], including an approach that takes as input a combination of observed values, missing data indicators, and the time intervals between observations. The time irregularity can also be captured by modifying the forget gate of an LSTM [21], while a new time gate that regulates access to the hidden and cell state of the LSTM was designed in [19]. Another solution for handling irregularly sampled data is to incorporate the time gaps between observations directly into Recurrent Neural Networks (RNNs). One approach is to add the time gap Δ_t to the RNN input, which has been found to be susceptible to overfitting [18]. An alternative method is to introduce hidden states that decay over time, which has been proposed in several works as a viable solution [3, 2, 22].

Hidden states with an exponential decay can be employed to parameterize neural Hawkes processes and explicitly model observations via latent state changes at each observation event [17]. Many works focus on modeling time series by leveraging a latent continuous-time function described by a neural network representation of its gradient field. More specifically, a variational auto-encoder model, which utilizes a neural network decoder in combination with a latent ordinary differential equation (ODE) model, has been presented in [4]. Based on this approach, an ODE-RNN encoder that consists of a neural ODE part that models the hidden state dynamics and an RNN part that updates the hidden state has been proposed [24]. A continuous-time version of the Gated Recurrent Unit, GRU-ODE-Bayes, that models the input series via continuous ODE dynamics describing the evolution of the probability distribution of the data, has also been employed for the irregular and multivariate setting [6]. Finally, an alternative to Neural ODEs, Neural Controlled Differential Equations represent the continuous-time analogue of an RNN, which benefits from memory-efficient adjoint-based backpropagation across observations [14].

Attention mechanisms combined with time encodings, as an alternative to positional ones [32], have been proposed [30, 37, 31]. By extending attention with learnable time embeddings [35], the recently proposed Multi-Time Attention Network [27] learns to attend to observations at different time points by computing a similarity weighting using only the time embedding, similar to kernel-based interpolation, but with the time attention-based similarity kernel being learnable. Except for the optimization issues of RNNs, the conventional dot-product self-attention mechanism matches queries with keys without considering the surrounding context. At the same time, space complexity grows quadratically with the input length, leading to memory constraints and potential performance limitations.

The use of implicit neural representations for creating continuous data representations by encoding the input in the weights of a neural network has recently gathered interest [20, 29]. Our approach can be conceptualized as an implicit representation of the convolutional kernels since they are parameterized as learnable and continuous functions of time. In this study, the proposed time-parameterized convolutional layer (TPC) introduces time-varying convolutional kernels, allowing for more efficient representational learning of the time dependencies among partially-observed variables. We leverage several continuous time functions for extracting learnable time embeddings of the time intervals across different variables. The proposed architecture is carefully designed for interpolation and classification tasks on irregularly sampled time series.

3 The TPC Layer

In this section, we define the mathematical properties of the employed Time-Parameterized layer (TPC) and analytically explain a proposed framework for tasks involving irregularly sampled, partially observed and

multivariate time series.

3.1 Preliminaries

Convolution is a well-studied mathematical operation which has applications in many diverse scientific fields [1]. The convolution of two functions f and g , denoted by $f * g$, expresses how the shape of one is modified by the other.

Continuous convolution. If the domains of functions f and g are continuous, convolution is defined as the integral of the product of the two functions after one is reflected and shifted. Formally, given $f: \mathbb{R}^D \rightarrow \mathbb{R}$ and $g: \mathbb{R}^D \rightarrow \mathbb{R}$, the continuous convolution operation is defined as:

$$(f * g)(\mathbf{x}) = \int_{-\infty}^{\infty} f(\mathbf{y})g(\mathbf{x} - \mathbf{y})dy$$

Discrete convolution. In the real world, signals are discrete and finite. For functions f, g , defined over the support domain of finite integer set \mathbb{Z}^D and $\{-K, -K + 1, \dots, K - 1, K\}^D$, respectively, the discrete equivalent of convolution is defined as:

$$(f * g)[n] = \sum_{k=-K}^K f[n - k]g[k] \quad (1)$$

Thus, the integral is replaced by a finite summation. Standard CNN models consist of layers that perform discrete convolutions that are defined over the discrete domain.

3.2 Time-Parameterized 1D Convolutions

We first introduce the key notations behind the employed time-parameterized convolutions for irregular and multivariate time series and analyze their fundamental properties.

Irregular time series and standard CNNs. Let $\{\mathbf{X}^{(1)}, \dots, \mathbf{X}^{(N)}\}$ be a collection of multivariate time series where $\mathbf{X}^{(i)} \in \mathbb{R}^{m \times L}$ for all $i \in \{1, \dots, N\}$. Thus, each time series consists of m channels and has a length (i.e., number of observations) equal to L which corresponds to the observation times $\{t_1, t_2, \dots, t_L\}$. Let also $d(\cdot, \cdot)$ denote a function that measures the distance (in time) between observations of a single channel of the collection of time series. The convolution operation of standard CNNs assumes that consecutive observations are equally spaced across all samples, and thus, the weights of the different kernels of standard CNNs are fixed across all chunks of the time series. In other words, the summation in the right part of Equation (1) is performed over the elements of the same set for all n . Formally, we have that $d(\mathbf{X}_{i,j}^{(i)}, \mathbf{X}_{i,j+1}^{(i)}) = \tau$ holds for all $i \in \{1, \dots, m\}$, $j \in \{1, \dots, L - 1\}$ and $i, j \in \{1, \dots, N\}$ where N is the number of samples. However, the above does not necessarily hold in the case of irregularly sampled time series data. Indeed, irregularly sampled time series can have different numbers of observations across different dimensions as well as across different data examples. Thus, due to the assumptions it makes, the standard convolution operation of CNNs is not suitable for irregular time series data.

Time-parameterized convolutional kernels. To deal with the irregularity of time series, we propose to use time-parameterized kernels. Thus, instead of a fixed kernel that slides over the patches of the time series, we use a parameterized kernel whose components are functions of time. The kernel is also parameterized by the weights of a neural network. We constraint the size of the kernel to be equal to $2z + 1$ where $z \in \mathbb{N}_0$ where \mathbb{N}_0 denotes the set of natural numbers together with zero. Then, the elements of the kernel are constructed by some function $g(\theta, \Delta t)$ where θ denotes some trainable parameters and Δt denotes the distance (in time)

of the observation associated with some element of the kernel and the $z + 1$ -th observation. Formally, the convolution is defined as follows:

$$(f * g)(t) = \sum_{i=1}^{2z+1} f(t_i)g(\theta, t - t_i) = \sum_{i=1}^{2z+1} f(t_i)g(\theta, \Delta t_i) \quad (2)$$

where t_1, \dots, t_{2z+1} are the timestamps associated with the observations of the patch the kernel is applied to.

The function $g(\theta, \Delta t)$ is quite general and can have different forms. In this paper, we focus on interpretability and thus function $g(\theta, \Delta t): \mathbb{R}^5 \rightarrow \mathbb{R}$ is defined as follows:

$$g\left(\begin{bmatrix} \theta_1 & \theta_2 & \theta_3 & \theta_4 & \Delta t \end{bmatrix}^\top\right) = \theta_1 \left(\sigma\left(h(\theta_3 \cdot \Delta t + \theta_4)\right) + \theta_2 \right)$$

where $h: \mathbb{R} \rightarrow \mathbb{R}$ is a continuous function in \mathbb{R} and $\sigma: \mathbb{R} \rightarrow \mathbb{R}$ denotes some activation function (i.e., sigmoid, ReLU, etc.). Thus, to construct each element of the kernel, function g takes as input four trainable parameters (i.e., $\theta_1, \theta_2, \theta_3$ and θ_4) and the time difference between the current observation and the center observation of the patch. Function h is chosen such that inductive bias is injected into the model. This can allow the model to capture patterns that commonly occur in time series data and also make its internal operations more interpretable. For example, a function $h(x) = c$ where c is some constant would not be a good candidate for extracting useful features from the time series. On the other hand, we employ more informative functions which can capture useful properties of time series such as trend and seasonality. In particular, we employ the following ten functions:

1. $h_1(x) = x$	6. $h_6(x) = x^2$
2. $h_2(x) = \sin(x)$	7. $h_7(x) = x^3$
3. $h_3(x) = \cos(x)$	8. $h_8(x) = \sinh(x)$
4. $h_4(x) = \tan(x)$	9. $h_9(x) = \cosh(x)$
5. $h_5(x) = \exp(x)$	10. $h_{10}(x) = \tanh(x)$

Most of the time, trend is a monotonic function, and therefore, functions h_1, h_6 and h_7 are chosen to detect trend in time series. Seasonality is a typical characteristic of time series in which the data experiences regular and predictable changes that recur over a defined cycle. Functions h_2, h_3, h_9 and h_{10} are responsible for extracting features that take seasonality into account.

The approach presented above generates kernels for univariate time series. In the case of multivariate time series, different parameters are learned for the different components of the time series. Therefore, the four parameters ($\theta_1, \theta_2, \theta_3$ and θ_4) are replaced by vectors of dimension m , i.e., $\theta_1, \theta_2, \theta_3, \theta_4 \in \mathbb{R}^m$. Thus, function $g(\theta, \Delta t): \mathbb{R}^{4m+1} \rightarrow \mathbb{R}^m$ is computed by applying function $h(\cdot)$ pointwise to m different elements. Note that Δt is still a scalar since observation times are identical across all components of the series.

3.3 The Time-Parameterized Convolutional (TPC) Layer

Given a sample $\mathbf{X}^{(i)}$, its corresponding observation times $\{t_1, t_2, \dots, t_L\}$, and a time-parameterized function g , the kernel centered at the j -th observation (i.e., $\mathbf{X}_{:,j}^{(i)}$) is constructed as follows:

Patch	$\mathbf{X}_{:,j-K}^{(i)}$...	$\mathbf{X}_{:,j}^{(i)}$...	$\mathbf{X}_{:,j+K}^{(i)}$
Observation time	t_{j-K}	...	t_j	...	t_{j+K}
Difference in time	Δt_{j-K}	...	0	...	Δt_{j+K}
Kernel	$g(\theta, \Delta t_{j-K})$...	$g(\theta, 0)$...	$g(\theta, \Delta t_{j+K})$

Note that $\mathbf{X}_{:,j}^{(i)}$ denotes the j -th column of matrix $\mathbf{X}^{(i)}$. Once we construct the kernel, the output of the convolution is computed as follows:

$$c = \sum_{l=1}^m g(\boldsymbol{\theta}, \Delta t_{j-K})_l \mathbf{X}_{l,j-K}^{(i)} + \dots + \sum_{l=1}^m g(\boldsymbol{\theta}, 0)_l \mathbf{X}_{l,j}^{(i)} + \dots \\ + \sum_{l=1}^m g(\boldsymbol{\theta}, \Delta t_{j+K})_l \mathbf{X}_{l,j+K}^{(i)}$$

where $c \in \mathbb{R}$. In some cases, features of the multivariate time series might be missing. In such cases, the above operation would compute the sum of a smaller number of terms (since missing features are ignored). Thus, we also experimented with the mean function:

$$c = \frac{1}{\nu} \left(\sum_{l=1}^m g(\boldsymbol{\theta}, \Delta t_{j-K})_l \mathbf{X}_{l,j-K}^{(i)} + \dots + \sum_{l=1}^m g(\boldsymbol{\theta}, 0)_l \mathbf{X}_{l,j}^{(i)} + \dots \right. \\ \left. + \sum_{l=1}^m g(\boldsymbol{\theta}, \Delta t_{j+K})_l \mathbf{X}_{l,j+K}^{(i)} \right) \quad (3)$$

where ν denotes the actual number of features (out of the $(2K+1)m$ features, those that are not missing).

Thus, the convolution between a sequence of observations and the kernel outputs a real number. We use zero padding and apply the kernel to all observations and, therefore we obtain a vector $\mathbf{c} \in \mathbb{R}^L$. Furthermore, similar to standard CNNs, not a single kernel, but instead a collection of kernels is generated and applied to the input. These kernels might correspond to different functions of the ones defined above (i.e., h_1, \dots, h_{10}). Suppose that we use p different kernels in total (potentially of different functions). Then, the output of the TPC layer of the multivariate and irregularly sampled time series $\mathbf{X}^{(i)}$ is computed as:

$$TPC(\mathbf{X}^{(i)}, \mathbf{t}^{(i)}) = \|\mathbf{c}_i\|_{i=1}^p \in \mathbb{R}^{L \times p}$$

where $\|$ is the concatenation operator between vectors and $\mathbf{t}^{(i)}$ is a vector that stores the observation times of the time series.

3.4 Properties of TPC Layer

Constant number of parameters An interesting property of the TPC layer is that the number of parameters of each kernel is constant and equal to $4m$ regardless of the size of the kernel. This is because the kernel is dynamically generated based on the observation times and only $4m$ trainable parameters are involved. This is in contrast to standard convolutional layers where the number of parameters is equal to the size of the kernel plus the bias. Thus, the number of parameters of the TPC layer will be less than the number of parameters of a standard convolutional layer when the size of the kernels is greater than 4. This is likely to lead to less complex models and might significantly reduce overfitting.

Time Complexity. The time complexity of the proposed TPC layer is approximately $\mathcal{O}(L\ell mp)$ for kernel size ℓ , similar to the vanilla 1D convolution. Since TPC relies on convolutions, that take advantage of parallel computations, it can be trained faster than recurrent neural network architectures. The complexity comparison becomes even more advantageous when compared with continuous-time models, such as neural ODEs that are significantly slower than RNNs [14].

Learning Properties. The proposed TPC layer introduces time-varying convolutional kernels as opposed to fixed kernels that are commonly employed in traditional convolutional neural networks (CNNs). In other words, the employed kernels do not remain fixed throughout the whole length of the input series. This particular trait of TPC does not explicitly force weight sharing between different subsequences of the time

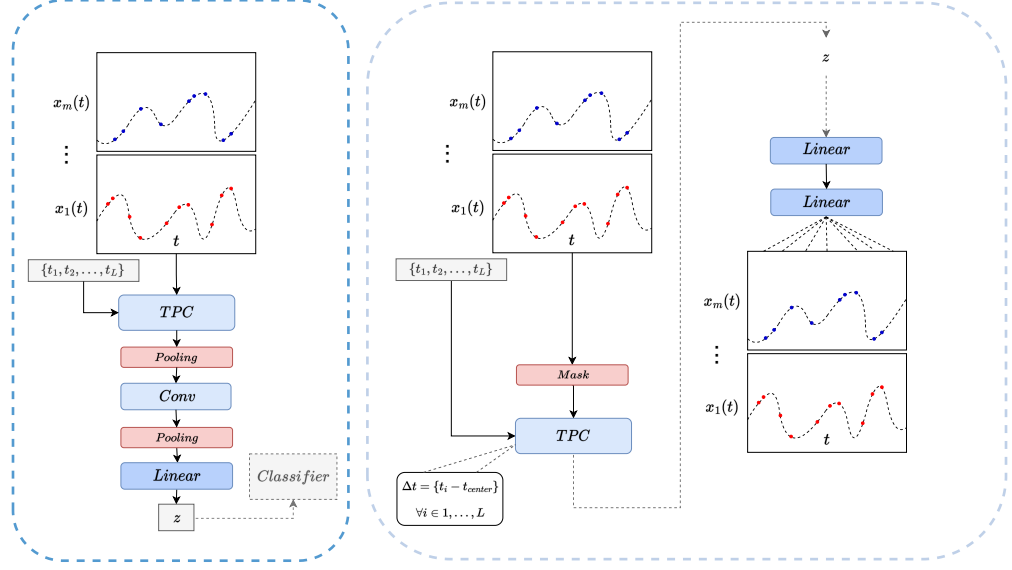


Figure 1: (Left) An encoder that consists of the proposed TPC layer, convolutions and pooling layer and produces a fixed-size latent representation z . (Right) An encoder-decoder framework that reconstructs the series from the input using TPC and linear layers.

series during convolution. Weight sharing is, however, implicitly modeled via the learnable representations of time, that are used to initialize the kernel weights. This is based on the assumption that observations that are mapped to similar time embeddings will probably share similar values of weights in the convolutional operation. The proposed approach still maintains the ability to locally aggregate information by retaining the notion of fixed kernel size in the convolution operation. This allows for the output of the convolution to be locally aggregated, while still incorporating the benefits of time-varying convolutional kernels.

Invariance Properties. If some patterns in the time series are identical, both in terms of the observations and also in terms of the difference in time between the observations, then the TPC layer will produce the same output for those two patterns. For example, let $\mathbf{x}_i = (x_{i-K}, \dots, x_i, \dots, x_{i+K})$ and $\mathbf{x}_j = (x_{j-K}, \dots, x_j, \dots, x_{j+K})$ denote two sequences of values and $\mathbf{t}_i = (t_{i-K}, \dots, t_i, \dots, t_{i+K})$ and $\mathbf{t}_j = (t_{j-K}, \dots, t_j, \dots, t_{j+K})$ denote their respective observation times. If $\mathbf{x}_i = \mathbf{x}_j$ holds and $\Delta\mathbf{t}_i = \Delta\mathbf{t}_j$ also holds, where $\Delta\mathbf{t}_i = (t_{i-K} - t_i, \dots, 0, \dots, t_{i+K} - t_i)$ and $\Delta\mathbf{t}_j = (t_{j-K} - t_j, \dots, 0, \dots, t_{j+K} - t_j)$, then the kernels produced for these two sequences of values are identical and therefore, the layer produces the same output.

Furthermore, the different functions defined in the previous subsection make the kernels invariant to different transformations. For instance, in the above example, suppose that $\Delta\mathbf{t}_i \neq \Delta\mathbf{t}_j$, and that the k -th element of the second sequence is equal to $(k+1)2\pi$ times the corresponding element of the first sequence for $k \in \{0, 1, \dots, 2K+1\}$. Then, the TPC layer equipped with the h_2 function (i.e., $\sin(\cdot)$ function) and with $\theta_3 = 1$ and $\theta_4 = 0$ would produce the same output for both patterns. Such a function can capture periodic temporal correlations.

3.5 TPCNN Framework for Irregularly Sampled Time Series

We will next discuss how the TPC layer can be integrated into neural network architectures for dealing with various tasks that involve irregular time series, such as interpolation and classification. Following previous work, we propose an encoder-decoder framework, so-called Time-Parameterized Convolutional Neural Network

(TPCNN) framework. In what follows, we give more details about the two main components of the proposed framework, namely its encoder and its decoder.

TPCNN Encoder. This module is responsible for mapping the input time series into a latent vector which captures their overall shape and their specificities. The first layer of the encoder is an instance of the TPC layer introduced above. The TPC layer receives as input the irregular and multivariate series $\mathbf{X}^{(i)} \in \mathbb{R}^{m \times L}$ and the corresponding vector of observation times $\mathbf{t}^{(i)} = \{t_1, t_2, \dots, t_L\}$. The output of TPC layer is then successively fed to vanilla convolution layers which can capture longer-time dependencies of the continuous latent representation of the time series. A pooling layer follows each convolution layer, including TPC. By down-sampling the output, such layers are expected to extract features that are good indicators of class membership or of the shape of the time series. Finally, a fully-connected layer is applied to the output of the last convolution layer to extract a low-dimensional representation $\mathbf{z}^{(i)} \in \mathbb{R}^d$ of the series.

TPCNN Decoder. This part of the architecture is responsible for reconstructing the multivariate input series from the latent vector that is produced by the encoder. The latent vector \mathbf{z} that was produced by the encoder is first given as input to a fully-connected layer whose objective is to perform rescaling. The emerging vector is then passed onto another fully-connected layer which produces a matrix $\hat{\mathbf{X}}^{(i)}$ that matches the dimension of the input time series. These reconstructed time series are then compared against the input series to evaluate the autoencoder's performance.

Interpolation and Classification Setting. Note that some components of the TPCNN framework depend on the considered task, i. e., interpolation or classification. For instance, in the interpolation setting, each time a kernel of the TPC layer is applied to some subset of the input series, the observation that lies at the center of that subset is masked such that the model does not have direct access to it. On the other hand, such a masking is not performed in the case of the classification setting.

The reconstruction loss of a standard autoencoder is typically measured using the mean squared error (MSE) between the original input and the reconstructed output. For an input time series $\mathbf{X}^{(i)}$, the MSE loss is computed as:

$$\mathcal{L}_{interpolation} = \frac{1}{|\mathcal{O}|} \sum_{j \in \mathcal{O}} \|\mathbf{X}_{:,j}^{(i)} - \hat{\mathbf{X}}_{:,j}^{(i)}\|_2^2$$

where \mathcal{O} is a set that contains the indices of the observed values and $\hat{\mathbf{X}}^{(i)}$ denotes the reconstructed series produced by the decoder as a function of the latent vector \mathbf{z} .

The encoder-decoder framework of Figure 1 (Right) is combined with the MSE loss for the interpolation task. Additionally, as already discussed, masking is performed on the center element of each slice of the input series, and the rest of the observed values of the slice are used for interpolation.

In the case of classification, the latent representation \mathbf{z} that is generated by the encoder and which preserves the information about the multivariate time series' dependencies, can be directly fed to a classifier module to make predictions. In the experiments that follow, we employ a 2-layer multi-layer perceptron (MLP) with *ReLU* activation function. Thus, in the case of a classification problem with $|\mathcal{C}|$ classes, the output is computed as follows:

$$\mathbf{p} = softmax(MLP(\mathbf{z}))$$

Then, given a training set consisting of time series $\mathbf{X}^{(1)}, \dots, \mathbf{X}^{(N)}$, we use the negative log-likelihood of the correct labels as training loss:

$$\mathcal{L}_{classification} = - \sum_{i=1}^N \sum_{j=1}^{|\mathcal{C}|} \mathbf{y}_j^{(i)} \log \mathbf{p}_j^{(i)}$$

where $\mathbf{y}_j^{(i)}$ is equal to 1 if $\mathbf{X}^{(i)}$ belongs to the j -th class, and 0 otherwise.

The application of the TPCNN model to the above two scenarios is illustrated in Figure 1 (classification on the left and interpolation on the right).

4 Experiments

In this section, we describe the experimental setup and methodology used to evaluate the performance of our proposed time-parameterized convolutional layer on various tasks involving irregular time series, including interpolation and classification.

4.1 Datasets

We evaluate the performance of the proposed architecture and the baselines on the following real-world datasets:

PhysioNet: The PhysioNet Challenge 2012 dataset [28] comprises 8000 multivariate time series extracted from intensive care unit (ICU) records. Each record includes sparse and irregularly spaced measurements from the first 48 hours of a patient’s admission to the ICU and has 37 variables. The dataset is split into 4000 labeled and 4000 unlabeled instances, with 13.8% of examples being in the positive class (in-hospital mortality). For the interpolation experiments, we used all 8000 instances and for the classification experiments, we used the 4000 labeled instances. To conduct the experiments, we followed the procedures of [24] and rounded the observation times to the nearest minute, resulting in 2880 possible measurement times per time series.

MIMIC-III: The MIMIC-III dataset [13] consists of multivariate, sparse and irregularly sampled physiological signals collected at Beth Israel Deaconess Medical Center from 2001 to 2012. Following the procedures of [24], 53211 records each containing 12 physiological variables are extracted. Using the first 48 hours of data the task is to predict in-hospital mortality, with 8.1% of the instances in the positive class.

Human Activity: The human activity dataset contains time series data from five individuals performing various activities (such as walking, sitting, lying, standing, etc.), with 3D positions of tags attached to their belts, chest and ankles (12 features in total). Following the data preprocessing steps outlined by [24], a dataset of 6,554 sequences with 12 channels and 50 time points was constructed. The task for this is to classify each time point in the sequence into one of eleven types of activities.

4.2 Experimental Setting

We next explain the experimental setting we follow for interpolation and classification, similar to the work of [27]. We perform interpolation experiments on the 8000 instances in the PhysioNet dataset by dividing it into a training set (80%) and a test set (20%). A portion of the training data (20%) is used for validation. The interpolation task involves conditioning on a subset of available points and predicting values for the remaining time points. We perform experiments with varying percentages of observed points, ranging from 50% to 90% of the available points. During testing, the observed points were given as input to the model and the model is used to infer the values at the remaining available time points in the test set. The experiments are repeated five times using different random seeds for model parameter initialization. The performance is evaluated using the mean squared error (MSE).

We also use the labeled data from the PhysioNet, MIMIC-III and Human Activity datasets to conduct classification experiments. For the PhysioNet and MIMIC-III datasets classification is performed for the whole time series, whereas, for the human activity dataset, we classify each time point within the series. We randomly divide each data set into a training set, containing 80% of the time series, and a test set, containing the remaining 20% of instances. We use 20% of the training set for validation. We repeat each experiment five times using different random seeds to initialize the model parameters. To account for class imbalance in the PhysioNet and MIMIC-III datasets, we assess classification performance using the area under the ROC curve (AUC score). On the other hand, for the Human Activity dataset, we evaluate models using accuracy. We use the validation set in order to select the best set of hyperparameters for our models via grid

Table 1: Performance for interpolation with different percentages of observed time points on *PhysioNet*. We mention in bold the best-performing method(s) and underline the second best-performing method(s) based on statistical significance tests.

Model	Mean Squared Error ($\times 10^{-3}$)				
RNN-VAE	13.418 ± 0.008	12.594 ± 0.004	11.887 ± 0.007	11.133 ± 0.007	11.470 ± 0.006
L-ODE-RNN	8.132 ± 0.020	8.140 ± 0.018	8.171 ± 0.030	8.143 ± 0.025	8.402 ± 0.022
L-ODE-ODE	6.721 ± 0.109	6.816 ± 0.045	6.798 ± 0.143	6.850 ± 0.066	7.142 ± 0.066
mTAND-FULL	4.139 ± 0.029	4.018 ± 0.048	4.157 ± 0.053	4.410 ± 0.149	4.798 ± 0.036
TPCNN (OURS)	5.993 ± 0.058	5.797 ± 0.063	5.654 ± 0.108	5.624 ± 0.084	5.532 ± 0.140
Observed(%)	50%	60%	70%	80%	90%

search. Once we have determined the optimal set of hyperparameters, we use the corresponding model to make predictions on the test set.

4.3 Baseline Models

In this study, we conduct a thorough evaluation of several deep learning architectures as baseline models for performance comparison. These models are specifically designed to handle irregular time series and include variations of the Recurrent Neural Network (RNN), Attention modules and encoder-decoder architectures.

The specific models evaluated in this study include:

- (i) Basic RNN variants including: *RNN-Impute*, *RNN- Δ_t* , *RNN-decay*, *GRU-D*. The *RNN-Impute* model employs a method to impute missing data points by utilizing a weighted average of the last observed measurement within the same time series and the overall mean of the variable across all training examples [3]. In *RNN- Δ_t* the input is augmented with a masking variable and a time interval Δ_t for each missing variable. The *RNN-decay* is an RNN with hidden states that decay exponentially over time [18, 3], whereas *GRU-D* employs exponential decay on both hidden states and input [3].
- (ii) Other RNN variants, such as *Phased-LSTM*, *IP-Nets*, *SeFT*, *RNN-VAE*. The *Phased-LSTM* model incorporates time irregularity through the use of a time gate that controls access to the hidden and cell states of the LSTM [19] and also uses forward filling to address the issue of partially observed vectors. *IP-Nets* are Interpolation-Prediction Networks (IPN), which consist of multiple semi-parametric RBF interpolation layers and a GRU [26]. The *SeFT* model adopts a set function-based approach, where observations are modeled individually and then pooled together using an attention-based mechanism [11]. *RNN-VAE* is a standard variational RNN encoder-decoder.
- (iii) ODE variants, such as *ODE-RNN*, *L-ODE-RNN*, *L-ODE-ODE*. In *ODE-RNN* neural ODEs model the dynamics of the hidden state, and an RNN updates the hidden state in the presence of new observations [24]. Similarly, *L-ODE-RNN* and *L-ODE-ODE* are latent ODEs with the former combining an RNN encoder and a neural ODE decoder [4], and the latter an ODE-RNN encoder and a neural ODE decoder [24].
- (iv) Attention-based frameworks, including *mTAND*. The multi-time attention network, *mTAND*, learns an embedding of continuous time values and uses an attention mechanism to produce a fixed-length representation of a time series containing a variable number of observations [27].

4.4 Results

Interpolation of missing data. In Table 1 we present the results of the experimental setting designed for interpolation, as described in Section 4.2. For different percentages of observed values (i. e., ranging from 50%

Table 2: Performance for **per-sequence** classification on *PhysioNet* and *MIMIC-III* and **per-time-point** classification on *Human Activity* datasets. We mention in bold the best-performing method(s) and underline the second best-performing method(s) based on statistical significance tests.

Model	AUC		Accuracy Human Activity
	PhysioNet	MIMIC-III	
RNN-IMPUTE	0.764 ± 0.016	0.8249 ± 0.0010	0.859 ± 0.004
RNN- Δ_t	0.787 ± 0.014	0.8364 ± 0.0011	0.857 ± 0.002
RNN-DECAY	0.807 ± 0.003	0.8392 ± 0.0012	0.860 ± 0.005
RNN GRU-D	0.818 ± 0.008	0.8270 ± 0.0010	0.862 ± 0.005
PHASED-LSTM	<u>0.836 ± 0.003</u>	0.8429 ± 0.0035	0.855 ± 0.005
IP-NETS	0.819 ± 0.006	0.8390 ± 0.0011	0.869 ± 0.007
SEFT	0.795 ± 0.015	<u>0.8485 ± 0.0022</u>	0.815 ± 0.002
RNN-VAE	0.515 ± 0.040	0.5175 ± 0.0312	0.343 ± 0.040
ODE-RNN	<u>0.833 ± 0.009</u>	0.8561 ± 0.0051	0.885 ± 0.008
L-ODE-RNN	0.781 ± 0.018	0.7734 ± 0.0030	0.838 ± 0.004
L-ODE-ODE	<u>0.829 ± 0.004</u>	0.8559 ± 0.0041	0.870 ± 0.028
mTAND-FULL	0.858 ± 0.004	<u>0.8544 ± 0.0024</u>	0.910 ± 0.002
TPCNN (ours)	<u>0.833 ± 0.001</u>	0.8380 ± 0.0011	0.897 ± 0.004

Table 3: Memory and computational costs, in terms of size (number of parameters) and time per epoch (in minutes).

Model	PhysioNet	MIMIC-III	Human Activity
SIZE (PARAMETERS)			
mTAND-FULL	1.3M	1.4M	1.6M
TPCNN (ours)	350K	100K	300K
TIME PER EPOCH (min)			
mTAND-FULL	0.06	0.5	0.006
TPCNN (ours)	0.15	0.2	0.008

to 90%), we record the interpolation performance on the reconstructed irregularly sampled multivariate time series of the PhysioNet dataset using the MSE metric. We compare the proposed TPCNN model to different baseline methods designed for interpolation, including RNN-VAE, L-ODE-RNN, L-ODE-ODE and mTAND-Full (i.e., mTAND encoder-decoder framework for interpolation). We mention in bold the best-performing method and underline the results for the second-best-performing method. We also perform tests for measuring the statistical significance of the studied methods, which leads to highlighting two distinct models that refer to the highest performances. We can observe that the best-performing method is mTAND-Full, which is closely followed by the proposed TPCNN model. The rest of the baselines show significantly worse performance compared to the proposed TPCNN, including the highly accurate in the irregular setting ODE-based method L-ODE-ODE. The performance of the proposed model ranges from $\sim 6.0 \times 10^{-3}l$ to $\sim 5.5 \times 10^{-3}$ in terms of MSE, showing a slightly improved performance as the percentage of missing observations decreases. On the other hand, mTAND-Full shows a slightly degrading performance for a smaller percentage of missing data, with RNN-VAE being the only baseline method that follows the same behavior.

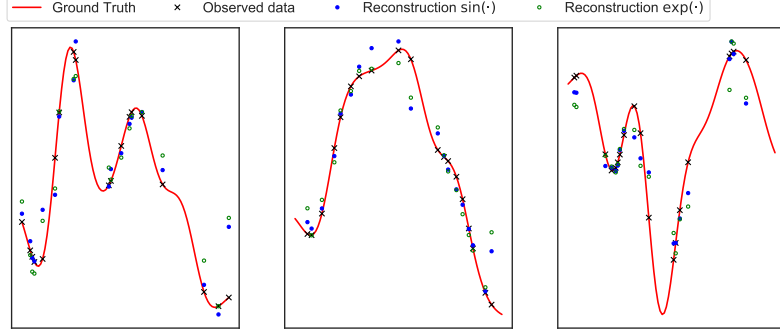


Figure 2: Reconstruction results using the proposed TPCNN model on the synthetic dataset. Three different samples of the test set are visualized.

Classification. We also report in Table 2 the results of the different baselines, as described in Section 4.3, and the proposed TPCNN model on classification for the labeled instances of PhysioNet, MIMIC-III and Human Activity datasets. For the first two imbalanced datasets, we use AUC as an evaluation metric and perform per-sequence binary classification, whereas, for the Human Activity dataset, we report accuracy for the task of per-time-point classification. For all datasets, we boldly mention the best-performing methods and underline the results for the second best-performing methods. Due to several non-statistically significant differences in performances, we have several methods being among the first or second best-performing. For PhysioNet and Human Activity datasets, our proposed TPCNN framework is the second-best method in terms of metrics, surpassed by the attention-based model mTAND-Full. More specifically, in PhysioNet the proposed model performs as well as the ODE variants (i. e., ODE-RNN, L-ODE-ODE) that are however significantly slow in terms of computational time, as mentioned in [27]. In Human Activity classification, TPCNN shows quite improved performance being $\sim 1\%$ worse than mTAND-Full. However, in the MIMIC-III classification, the proposed TPCNN model lies among the third-best-performing methods, being surpassed by several baselines. In this dataset, ODE-RNN, L-ODE-ODE and mTAND-Full methods achieve the highest AUC scores, followed by the SeFT model, which however performs significantly worse in classification experiments for the other two datasets. The significant performance advantage of mTAND-Full in this task can be attributed to its design which jointly performs interpolation and classification while directly attending only to observed time points. On the other hand, the proposed model handles missing data inside the convolutional kernel of the TPC layer by applying the mean aggregator of Equation 3. The aggregation neighborhood however is constrained by the kernel size and remains fixed throughout the series length. Extending the proposed architecture to incorporate size-varying kernels could further improve the learning capabilities of the TPC layer.

Computational cost. In Table 3 we provide a comparison in terms of memory and computational costs between the proposed TPCNN and its main competitor mTAND-Full. We report the size, i. e., the number of parameters, and the time per epoch in minutes for the two methods and the three real-world datasets. Comparisons of mTAND and previous state-of-the-art models, among which the efficient ODE-based methods, as shown in [27] have demonstrated that the former is significantly faster (i. e., approximately 100 times) than ODE-based methods that make use of an ODE solver. As we can observe in Table 3, TPCNN is as fast as mTAND-Full in terms of time cost comparison. When it comes to the size of the model, the proposed TPCNN uses significantly fewer parameters compared to mTAND-Full, while maintaining competitive performance. More specifically, TPCNN uses approximately some hundred thousand parameters, i. e., 100 – 350 thousand parameters, while mTAND-Full size scales to millions of parameters, i. e., approximately 1.5 million. This comparison highlights the high efficacy of convolutions in the irregular sampling setting, which allow the training of neural networks that are significantly smaller and fast compared to the baselines. Therefore, the

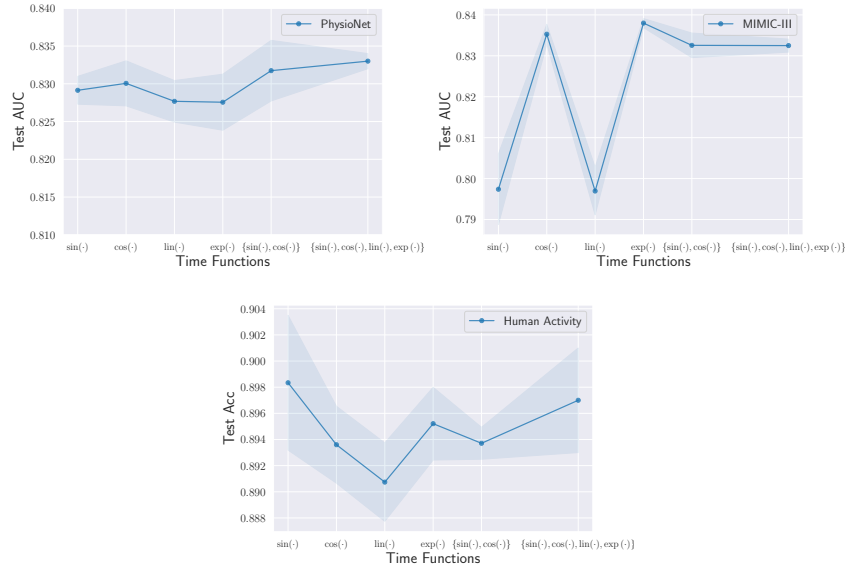


Figure 3: Ablation study on different time functions for the parameterization of convolutional kernels for each dataset. Each plot captures the performance (AUC or Accuracy) for each function or combination of functions on the test set.

proposed TPCNN can easily scale to larger datasets and remains efficient even when trained with fewer parameters.

Experiments on synthetic data. Following the line of work of [27], we reproduce their synthetic sinusoidal dataset that consists of 1000 samples, each describing a time series of 100 time points where $t \in [0, 1]$. Given 10 reference points, an RBF kernel with bandwidth 100 is used to obtain local interpolations at the 100 time steps. For each sample, 20 time points are randomly selected so as to represent an irregularly spaced series. We use 80% of the dataset for training and the rest 20% for testing. We employ the encoder-decoder interpolation framework of Figure 1 (Right). Contrary to the interpolation setting for PhysioNet, we give as input the 20 irregular time steps, without the missing points, and reconstruct each observation based on the rest using TPCNN with the functions $h_2(x) = \sin(x)$ (blue points) and $h_5(x) = \exp(x)$ (green points). We visualize the obtained reconstructions for 3 samples of the test set in Figure 2. Each plot consists of the true values (ground truth) for a test sample, while the dark markers represent the 20 observed input data points (observed data), the blue markers and the green markers the 20 predicted values (reconstruction) using $\sin(\cdot)$ and $\exp(\cdot)$ functions respectively. By employing the function $h_2(x) = \sin(x)$, we are able to achieve a lower MSE loss compared to the ones achieved with the rest of the time functions defined in Section 3.2. We should mention here that in case domain knowledge is available, it can be incorporated into the proposed TPCNN method via the employed time function, which is likely to lead to performance improvements.

Ablation study. We also present in Figure 3 an ablation study on different time functions employed for parameterizing the weights of the convolutional kernels. The performance metric (AUC or accuracy) on the test set is reported on the classification task of the real-world datasets given a different time function or combination of time functions. For all three datasets, we examine a subset of the functions described in Section 3.2. More specifically, we employ $h_1(x), h_2(x), h_3(x), h_5(x)$ (i.e., $\text{lin}(\cdot), \sin(\cdot), \cos(\cdot), \exp(\cdot)$) and their combination (e.g., $\{\sin(\cdot), \cos(\cdot)\}, \{\sin(\cdot), \cos(\cdot), \text{lin}(\cdot), \exp(\cdot)\}$). We observe that different functions may contribute more or less to the classification performance for the given dataset. In PhysioNet, while the linear function $\text{lin}(\cdot)$ and exponential function $\exp(\cdot)$ lead to the lowest AUC on the test set, when combined with

$\sin(\cdot)$ and $\cos(\cdot)$ they achieve a performance improvement by $\sim 1\%$. Additionally, in MIMIC-III classification $\cos(\cdot)$ and $\exp(\cdot)$ functions show the highest AUC test, while $\sin(\cdot)$ and $\text{lin}(\cdot)$ (i.e., linear function) lead to a reduced performance by $\sim 4\%$. At the same, the combination of functions improves performance but does not surpass $\cos(\cdot)$ and $\exp(\cdot)$ when employed alone. Finally on the Human Activity dataset, $\cos(\cdot)$ function and the combination $\{\sin(\cdot), \cos(\cdot), \text{lin}(\cdot), \exp(\cdot)\}$, followed by the $\exp(\cdot)$ function achieve the highest test accuracy. The linear $\text{lin}(\cdot)$ function again, in this case, leads to the lowest accuracy score compared to the rest of the time functions. During training, we can observe that the linear time function followed by a standard non-linear activation (e.g., ReLU) when used for the parameterization of the convolutional kernel weights suffers from slow convergence and consequently worse performance. On the other hand, periodic time functions and the exponential function seem to more efficiently describe the time dynamics and lead to smoother training when used for parameterizing convolutions. This experiment highlights the explainability aspects of the proposed TPCNN model since it allows us to determine which time functions better describe the considered time series. Furthermore, under certain conditions, the time series could be considered as a composition of such kind of functions.

5 Conclusion

In this work, we carefully designed and experimentally evaluated a novel time-parameterized convolutional neural network, which incorporates learnable time functions into the weights of convolutional kernels. The proposed method generalizes well in different tasks involving irregularly sampled multivariate time series while being computationally efficient and interpretable.

References

- [1] E Oran Brigham. *The fast Fourier transform and its applications*. Prentice-Hall, Inc., 1988.
- [2] Wei Cao, Dong Wang, Jian Li, Hao Zhou, Lei Li, and Yitan Li. Brits: Bidirectional recurrent imputation for time series. *Advances in neural information processing systems*, 31, 2018.
- [3] Zhengping Che, Sanjay Purushotham, Kyunghyun Cho, David Sontag, and Yan Liu. Recurrent neural networks for multivariate time series with missing values. *Scientific reports*, 8(1):1–12, 2018.
- [4] Ricky TQ Chen, Yulia Rubanova, Jesse Bettencourt, and David Duvenaud. Neural ordinary differential equations. In *Advances on Neural Information Processing Systems*, pages 6572–6583, 2018.
- [5] Junyoung Chung, Caglar Gulcehre, KyungHyun Cho, and Yoshua Bengio. Empirical evaluation of gated recurrent neural networks on sequence modeling. *arXiv preprint arXiv:1412.3555*, 2014.
- [6] Edward De Brouwer, Jaak Simm, Adam Arany, and Yves Moreau. Gru-ode-bayes: Continuous modeling of sporadically-observed time series. *Advances in neural information processing systems*, 32, 2019.
- [7] Jan G De Gooijer and Rob J Hyndman. 25 years of time series forecasting. *International Journal of Forecasting*, 22(3):443–473, 2006.
- [8] Cristóbal Esteban, Stephanie L Hyland, and Gunnar Rätsch. Real-valued (medical) time series generation with recurrent conditional gans. *arXiv preprint arXiv:1706.02633*, 2017.
- [9] Joseph Futoma, Sanjay Hariharan, and Katherine Heller. Learning to detect sepsis with a multitask gaussian process rnn classifier. In *International conference on machine learning*, pages 1174–1182. PMLR, 2017.
- [10] Sepp Hochreiter and Jürgen Schmidhuber. Long short-term memory. *Neural computation*, 9(8):1735–1780, 1997.

[11] Max Horn, Michael Moor, Christian Bock, Bastian Rieck, and Karsten Borgwardt. Set functions for time series. In *International Conference on Machine Learning*, pages 4353–4363. PMLR, 2020.

[12] Hassan Ismail Fawaz, Germain Forestier, Jonathan Weber, Lhassane Idoumghar, and Pierre-Alain Muller. Deep learning for time series classification: a review. *Data mining and knowledge discovery*, 33(4):917–963, 2019.

[13] Alistair EW Johnson, Tom J Pollard, Lu Shen, Li-wei H Lehman, Mengling Feng, Mohammad Ghassemi, Benjamin Moody, Peter Szolovits, Leo Anthony Celi, and Roger G Mark. Mimic-iii, a freely accessible critical care database. *Scientific data*, 3(1):1–9, 2016.

[14] Patrick Kidger, James Morrill, James Foster, and Terry Lyons. Neural controlled differential equations for irregular time series. *Advances in Neural Information Processing Systems*, 33:6696–6707, 2020.

[15] Yann LeCun, Léon Bottou, Yoshua Bengio, and Patrick Haffner. Gradient-based learning applied to document recognition. *Proceedings of the IEEE*, 86(11):2278–2324, 1998.

[16] Yonghong Luo, Xiangrui Cai, Ying Zhang, Jun Xu, et al. Multivariate time series imputation with generative adversarial networks. *Advances in neural information processing systems*, 31, 2018.

[17] Hongyuan Mei and Jason M Eisner. The neural hawkes process: A neurally self-modulating multivariate point process. *Advances in neural information processing systems*, 30, 2017.

[18] Michael C Mozer, Denis Kazakov, and Robert V Lindsey. Discrete event, continuous time rnns. *arXiv preprint arXiv:1710.04110*, 2017.

[19] Daniel Neil, Michael Pfeiffer, and Shih-Chii Liu. Phased lstm: Accelerating recurrent network training for long or event-based sequences. *Advances in neural information processing systems*, 29, 2016.

[20] Jeong Joon Park, Peter Florence, Julian Straub, Richard Newcombe, and Steven Lovegrove. Deepsdf: Learning continuous signed distance functions for shape representation. In *Proceedings of the IEEE/CVF conference on computer vision and pattern recognition*, pages 165–174, 2019.

[21] Trang Pham, Truyen Tran, Dinh Phung, and Svetha Venkatesh. Predicting healthcare trajectories from medical records: A deep learning approach. *Journal of biomedical informatics*, 69:218–229, 2017.

[22] Alvin Rajkomar, Eyal Oren, Kai Chen, Andrew M Dai, Nissan Hajaj, Michaela Hardt, Peter J Liu, Xiaobing Liu, Jake Marcus, Mimi Sun, et al. Scalable and accurate deep learning with electronic health records. *NPJ digital medicine*, 1(1):1–10, 2018.

[23] David W Romero, Anna Kuzina, Erik J Bekkers, Jakub M Tomczak, and Mark Hoogendoorn. Ckconv: Continuous kernel convolution for sequential data. *arXiv preprint arXiv:2102.02611*, 2021.

[24] Yulia Rubanova, Ricky TQ Chen, and David K Duvenaud. Latent ordinary differential equations for irregularly-sampled time series. *Advances in neural information processing systems*, 32, 2019.

[25] Kristof Schütt, Pieter-Jan Kindermans, Huziel Enoc Sauceda Felix, Stefan Chmiela, Alexandre Tkatchenko, and Klaus-Robert Müller. Schnet: A continuous-filter convolutional neural network for modeling quantum interactions. *Advances in neural information processing systems*, 30, 2017.

[26] Satya Narayan Shukla and Benjamin M Marlin. Interpolation-prediction networks for irregularly sampled time series. *arXiv preprint arXiv:1909.07782*, 2019.

[27] Satya Narayan Shukla and Benjamin M Marlin. Multi-time attention networks for irregularly sampled time series. *arXiv preprint arXiv:2101.10318*, 2021.

[28] Ikaro Silva, George Moody, Daniel J Scott, Leo A Celi, and Roger G Mark. Predicting in-hospital mortality of icu patients: The physionet/computing in cardiology challenge 2012. In *2012 Computing in Cardiology*, pages 245–248. IEEE, 2012.

[29] Vincent Sitzmann, Julien Martel, Alexander Bergman, David Lindell, and Gordon Wetzstein. Implicit neural representations with periodic activation functions. *Advances in Neural Information Processing Systems*, 33:7462–7473, 2020.

[30] Huan Song, Deepta Rajan, Jayaraman Thiagarajan, and Andreas Spanias. Attend and diagnose: Clinical time series analysis using attention models. In *Proceedings of the AAAI conference on artificial intelligence*, volume 32, 2018.

[31] Qingxiong Tan, Mang Ye, Baoyao Yang, Sici Liu, Andy Jinhua Ma, Terry Cheuk-Fung Yip, Grace Lai-Hung Wong, and PongChi Yuen. Data-gru: Dual-attention time-aware gated recurrent unit for irregular multivariate time series. In *Proceedings of the AAAI Conference on Artificial Intelligence*, volume 34, pages 930–937, 2020.

[32] Ashish Vaswani, Noam Shazeer, Niki Parmar, Jakob Uszkoreit, Llion Jones, Aidan N Gomez, Łukasz Kaiser, and Illia Polosukhin. Attention is all you need. *Advances in neural information processing systems*, 30, 2017.

[33] Shenlong Wang, Simon Suo, Wei-Chiu Ma, Andrei Pokrovsky, and Raquel Urtasun. Deep parametric continuous convolutional neural networks. In *Proceedings of the IEEE conference on computer vision and pattern recognition*, pages 2589–2597, 2018.

[34] Paul J Werbos. Backpropagation through time: what it does and how to do it. *Proceedings of the IEEE*, 78(10):1550–1560, 1990.

[35] Da Xu, Chuanwei Ruan, Evren Korpeoglu, Sushant Kumar, and Kannan Achan. Self-attention with functional time representation learning. *Advances in neural information processing systems*, 32, 2019.

[36] Jinsung Yoon, William R Zame, and Mihaela van der Schaar. Estimating missing data in temporal data streams using multi-directional recurrent neural networks. *IEEE Transactions on Biomedical Engineering*, 66(5):1477–1490, 2018.

[37] Yuan Zhang. Attain: Attention-based time-aware lstm networks for disease progression modeling. In *In Proceedings of the 28th International Joint Conference on Artificial Intelligence (IJCAI-2019)*, pp. 4369–4375, Macao, China., 2019.